



Cite this: DOI: 10.1039/d0nr00750a

Received 28th January 2020,
Accepted 19th March 2020

DOI: 10.1039/d0nr00750a
rsc.li/nanoscale

Nanoengineered immunosuppressive therapeutics modulating M1/M2 macrophages into the balanced status for enhanced idiopathic pulmonary fibrosis therapy†

Xin Chang,^{‡a} Lei Xing,^{‡a,b,c,d} Yi Wang,^a Tian-Jiao Zhou,^a Li-Jun Shen^a and Hu-Lin Jiang^{‡*a,b,c,d}

Effective treatment in clinic for idiopathic pulmonary fibrosis (IPF) remains a challenge due to low drug accumulation in lungs and imbalanced polarization of pro/anti-inflammatory macrophages (M1/M2 macrophages). Herein, a novel endogenous cell-targeting nanoplatform (PNCE) is developed for enhanced IPF treatment efficacy through modulating M1/M2 macrophages into the balanced status to suppress fibroblast over-activation. Notably, PNCE loaded with nintedanib (NIN) and colchicine (COL) can firstly target endogenous monocyte-derived multipotent cells (MOMCs) and then be effectively delivered into IPF lungs due to the homing ability of MOMCs, and detached sensitively from MOMCs by matrix metalloproteinases-2 (MMP-2) over-expressed in IPF lungs. After PNCE selectively accumulated within fibrosis foci, COL can mildly modulate the polarization of M1 macrophages into M2 macrophages to balance innate immune responses, which can enhance the suppressing effect of NIN on fibroblast activation, further improving the IPF therapy. Altogether, PNCE has two collaborative steps including the inhibition of innate immune responses accompanied by the decrease of fibroblast populations in IPF lungs, achieving a stronger and excellent anti-fibrotic efficacy both *in vitro* and *in vivo*. This endogenous cell-based engineered liposomal nanoplatform not only allows therapeutic drugs to take effect selectively *in vivo*, but also provides an alternative strategy for an enhanced curative effect by modulating innate immune responses in IPF therapy.

1. Introduction

Idiopathic pulmonary fibrosis (IPF) is a chronic lung parenchyma injury disease with a median survival time of 2–3 years, while the full recovery from IPF remains a huge challenge for clinical therapies.^{1,2} The main drawbacks of such therapies are that they can only help relieve symptoms, but not cut off the disease progression.^{3–5} Recently, nintedanib (NIN) was approved for IPF therapy by inhibiting fibroblast activation and the secretion of collagen to delay the IPF progression.^{6–8} However, the efficacy of NIN is limited on account of its inability to cut off innate immune responses that produce inflammatory factors such as interleukin 1 β (IL-1 β) and transforming growth factor beta (TGF- β), which accelerate re-proliferation of fibroblasts and aggravate IPF.^{9,10} Hereinto, a marked heterogeneity of the activation of pro-inflammatory macrophages (M1 macrophages) plays an important role in activating a wound-healing response by releasing inflammatory factors, which upregulate the activation of innate immune responses in IPF.^{2,11–13} In addition, the quiescent precursor fibroblasts are also activated by these inflammatory factors and then transform to myofibroblasts, which can produce an excessive extracellular matrix (ECM) and destroy normal tissue architecture.^{14,15} In brief, these excessive M1 macrophages play a dominant role in IPF progression, and inhibiting their excessive proliferation is a promising strategy to enhance anti-fibrosis therapy.

To date, some immune-regulators have also been exploited for treating IPF, such as colchicine (COL)¹⁶ which suppresses the expression of nuclear factor kappa B (NF- κ B) and extracellular regulated protein kinases 1/2 (ERK 1/2) involved in the polarization of M1 macrophages into anti-inflammatory macrophages (M2 macrophages), and blocks the release of pro-inflammatory cytokines, such as IL-1 β and TGF- β .¹⁷ However, using COL alone remains a challenge because IPF is considered as an inflammatory overactivated disease accompanied by establishing fibrosis. Meanwhile, effective delivery of immune regulators to injured lung tissues has not

^aState Key Laboratory of Natural Medicines, China Pharmaceutical University, 210009, China. E-mail: jianghulin3@163.com

^bJiangsu Key Laboratory of Druggability of Biopharmaceuticals, China Pharmaceutical University, 210009, China

^cJiangsu Key Laboratory of Drug Screening, China Pharmaceutical University, 210009, China

^dJiangsu Key Laboratory of Drug Discovery for Metabolic Diseases, China Pharmaceutical University, 210009, China

†Electronic supplementary information (ESI) available. See DOI: 10.1039/d0nr00750a

‡These authors contributed equally to this work.

been developed. Consequently, there is a great demand for development of an efficient lung targeted and enhanced strategy for modulating macrophage polarization to improve the anti-fibrosis efficacy.

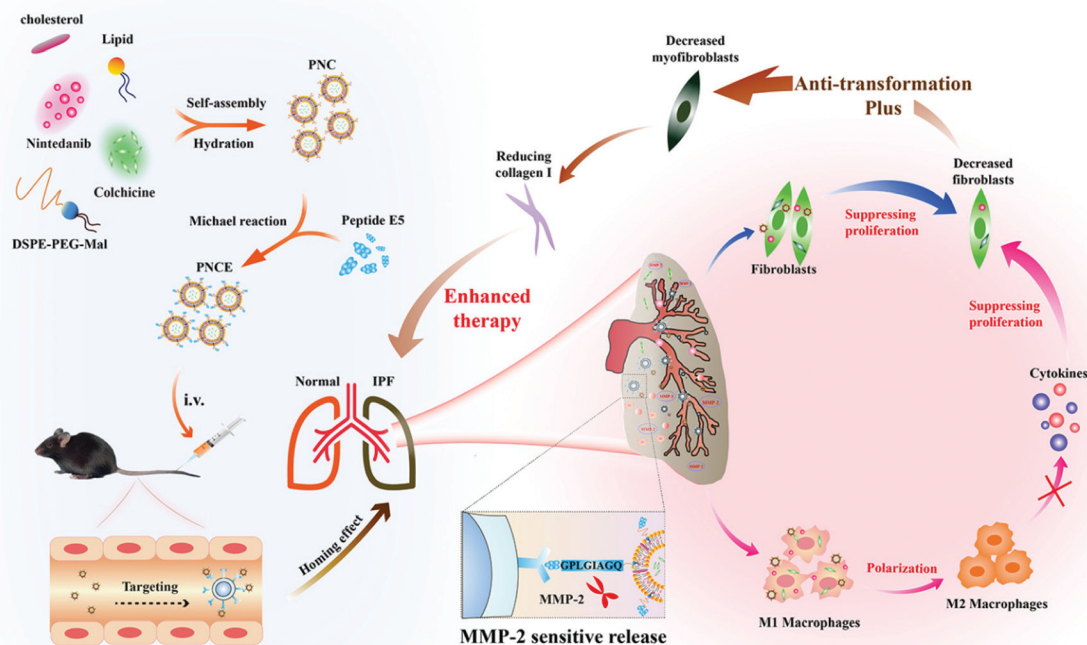
Herein, we employed novel and matrix metalloproteinase-2 (MMP-2) responsive peptide (peptide E5) modified engineered liposomes (PNCE) for IPF therapy. The peptide E5 is a straight chain consisting of amino acid residues, containing two components with an MMP-2 specific cleavable sequence and CXC chemokine receptor 4 (CXCR 4) targeting part, which can specifically target CXCR 4 overexpressed on the cell surface, and pathologically responsive fracture in MMP-2 overexpressed tissues.^{18,19} In this study, the PNCE could target monocyte-derived multipotent cells (MOMCs) forming programmed therapeutics (MOMCs@PNCE) to improve the accumulation of therapeutic drugs into IPF lungs, significantly inhibiting fibroblast re-activation by modulating the M1/M2 macrophage balance in the innate immune environment, and further enhancing the efficacy of IPF treatment (Scheme 1). After intravenous injection, PNCE could firstly adhere to the MOMCs by the targeting ability of peptide E5 to MOMCs in the blood circulation and be reprogrammed into MOMCs@PNCE as an engineered delivery platform, which could efficiently deliver the dual drugs to IPF lung tissues owing to the migration of MOMCs by chemokines to the IPF lungs and specifically release PNCE at the fibrotic site responding to the excessive deposition of MMP-2 by myofibroblasts.²⁰ COL was chosen as

an immunity regulator to balance innate immune responses by downregulating the M1 macrophage proportion and reducing the expression of inflammatory factors, which was the prerequisite for efficiently inhibiting the fibroblast proliferation, and NIN was an anti-fibrotic enhancer to block fibroblast activation. Hence, the combination of two drugs sheds light on the way to fight against IPF. The endogenous cell-based co-delivery nanoplatform offers a promising strategy which can increase the accumulation of dual drugs in IPF lungs, and also provides a practical scheme by modulating innate immune responses and synergistically inhibiting the fibroblast proliferation as an effective therapeutic strategy to improve the efficacy of IPF treatment.

2. Experimental

Materials

Cholesterol was purchased from Sinopharm Chemical Reagent Co., Ltd (Shanghai, China). Soybean phospholipids, 1,2-distearoyl-sn-glycero-3-phosphoethanolamine polyethylene glycol-maleimide, 2000 Da (DSPE-PEG2K-Mal) and DSPE-PEG2K were purchased from A.V.T. Pharmaceutical Co., Ltd (Shanghai, China). The peptide E5 was synthesized by Top-peptide Biotechnology Co., Ltd (Shanghai, China). NIN was purchased from Shanghai Yuanye Bio-Technology Co., Ltd (Shanghai, China). COL was purchased from J&K Scientific Co., Ltd



Scheme 1 Scheme depicting the inhibition of cytokines and improvement of the anti-fibrosis therapy effect of NIN *in vivo* by using the PNCE. The PNCEs target MOMCs and accumulate in lung tissue after intravenous injection, owing to the migration ability of MOMCs. Then, the PNCE is endocytosed by the cells and NIN and COL are released via lysosomes. COL inhibits macrophage proliferation and decreases cytokine secretion like IL-1 β . NIN can inhibit the population of fibroblasts, further reducing collagen deposition to enhance IPF therapy.

(Beijing, China). MMP-2 and the reactive oxygen species (ROS) probe 2',7'-dichlorofluorescein diacetate (DCFH-DA) were purchased from Sigma-Aldrich (St Louis, USA). Alpha smooth muscle actin (α -SMA) mouse monoclonal was purchased from Abcam (Massachusetts, USA). Lyso-Tracker Red DND-99 kit was purchased from Thermo Fisher (Waltham, USA). Ilomostat was purchased from Selleck (Houston, USA). 1,1'-Dioctadecyl-3,3,3',3'-tetramethylindotricarbocyanine iodide (DiR iodide) and 1,1'-dioctadecyl-3,3,3',3'-tetramethylindocarbocyanine perchlorate (DiI) were obtained from Fanbo Biochemicals Co., Ltd (Beijing, China). 3,3'-Dioctadecyloxycarbocyanine perchlorate (DiO) was purchased from Beyotime Co., Ltd (Shanghai, China). Dichloromethane was purchased from Wuxi Yasheng Chemical Co., Ltd (Wuxi, China). Lipopolysaccharide (LPS) and TGF- β were purchased from Multi Sciences Biotech Co., Ltd (Hangzhou, China). Bleomycin (BLM) sulfate was purchased from Zhejiang Huahai Pharmaceutical Co., Ltd (Linhai, China). Fetal bovine serum (FBS), 4,6-diamino-2-phenylindole (DAPI), Roswell park memorial institute 1640 (RPMI-1640) and bicinchoninic acid (BCA) protein assay kit were purchased from KeyGEN Biotech Co., Ltd (Nanjing, China). Lymphocyte isolation kit was purchased from Solarbio biotech Co., Ltd (Beijing, China). 3-(4,5-Dimethylthiazol-2-yl)-2,5-diphenyltetrazolium bromide (MTT) was purchased from J&K (Beijing, China). The other antibodies not mentioned were purchased from Servicebio Co., Ltd (Nanjing, China). The solvents were purchased from Aladdin (Shanghai, China).

Animals

C57BL/6 mice (male, 8 weeks old, ~20 g) were purchased from East China Normal University (Shanghai, China). All the animal study and handling procedures were according to the guidelines evaluated and approved by the regional ethics committee of China Pharmaceutical University (no. 26 Rev. 2016, Nanjing, China). Animals were acclimatized for 1 week, and then randomly divided into groups of 5 under a 12 h light/dark cycle, and allowed food and water freely.

BLM-induced IPF model: 8 weeks-old male C57BL/6 mice (~20 g) were anesthetized by intraperitoneal injection of chloralhydrate (250 mg kg⁻¹). The IPF mice model was injected with BLM solution (2 USP per kg)¹⁵ by endotracheal administration with endotracheal tubes in the BIOLITE intubation system (Braintree Scientific Inc., USA). The procedure of building an IPF model according to the manufacturer's protocols involved pulling out the tongues of the anesthetized mice firstly, and then finding the trachea with a lighting device, inserting an endotracheal tube and injecting a BLM solution.

Isolation and incubation of primary macrophages and lung fibroblasts

IPF mice (21 days after injection of BLM) were anesthetized and sacrificed, and then sterilized with 75% alcohol in a sterile counter. The lung tissues were harvested, and then washed with PBS and ground with RPMI-1640 media in a Petri dish. The tissues were then digested using collagenase IV (1 mg ml⁻¹) and trypsin (0.25%) in PBS at 37 °C for 1 h. The

lung cells were collected by centrifugation (1000 rpm, 5 min). **Macrophages:** the collecting lung cells were re-suspended with RPMI-1640 media and incubated into T-25. The macrophages were isolated from other lung cells according to different cell diameters. Macrophages were about 25 μ m in diameter. We first removed bits of lung tissues using a sterile filtration membrane of 150 μ m, then most epithelial cells were removed with a 50–60 μ m filter membrane, and macrophages were finally purified with a 30 μ m filter membrane for further culture. The macrophages were cultured in RPMI-1640 media with 10% FBS and the macrophages were incubated at 37 °C and 5% CO₂. **Fibroblasts:** The collecting lung cells were re-suspended with RPMI-1640 media and incubated into T-25. The lung fibroblasts were isolated from other lung cells depending on their differential adherent properties. After incubation for 30 min, the lung fibroblasts would adhere onto the Petri dish, and then non-adherent cells were removed. The cells were then cultured in culture media. The lung fibroblast cells were cultured in RPMI-1640 media with 10% FBS and lung fibroblasts were incubated at 37 °C and 5% CO₂.

Preparation of the PNCE, PNC and PN nano-formulation

NIN and COL loaded into a liposome platform were prepared by using the film dispersion method. Specifically, NIN (5 mg), soybean lecithin (80 mg), cholesterol (10 mg) and DSPE-PEG-Mal (10 mg) were dissolved in 5 mL dichloromethane and mixed in a 50 mL round bottom flask. The solvent was rotary evaporated at 45 °C for 20 min. Then 3 mL deionized water with COL (1 mg) was added and mixed by ultrasonic vibration for 30 min at 45 °C. After that, the peptide E5 (5 mg) was added into the above solution to obtain PNCE. Similarly, the preparation method of other formulations was the same as that of PNCE. The only difference was that DSPE-PEG (10 mg) rather than DSPE-PEG-Mal was soluble in dichloromethane. The Mal of DSPE-PEG-Mal was the crucial part of targeting MOMCs for further research. The preparation schemes of the PNC and PN were the same as mentioned above.

Ultraviolet-visible spectrophotometry (UV-vis) for drug determination

The absorbance was detected by UV-vis analysis between 200 and 500 nm, and the curves of NIN and COL were established. For determination of the absorbance of dual drugs in PNCE, 40 μ L PNCE solution was dissolved in 3960 μ L acetone and then measured at 200–500 nm by UV-vis. The drug encapsulated efficiency (EE) was as follows, W_1 represented the quality of encapsulated drugs and W_2 represented the quality of whole drugs: $EE (\%) = (W_1/W_2) \times 100\%$. The loading efficiency (LE) was as follows, W represented the quality of the whole reagent including materials and the added drugs: $LE (\%) = (W_1/W) \times 100\%$.

Reversed-phase high performance liquid chromatography (RP-HPLC) analysis

The standard curves of NIN and COL were acquired by HPLC. The standard solution of NIN and COL was dissolved in di-

chloromethane. An Agilent Technologies 1220 Infinity II LC was used to fit with an Ultimate XB-C18, 5 μm , 250 \times 4.6 mm column. The method involved a mobile phase of 0.1% trifluoroacetic acid : methyl alcohol, 10 : 90 (v/v), and the absorbance was detected by UV-vis analysis at 350 nm (COL) and 391 nm (NIN).

Isolation and incubation of MOMCs

IPF mice (21 days after injection of BLM) were anesthetized by intraperitoneal injection of 10% chloralhydrate solution (250 mg kg^{-1}). To obtain the MOMCs, peripheral blood was collected from the C57BL/6J mice with Ethylene Diamine Tetraacetic Acid (EDTA) and diluted 3 times with PBS. The isolated protocol of MOMCs was conducted according to a lymphocyte isolation kit. The MOMCs were cultured in RPMI-1640 media with 10% FBS and the macrophages were incubated at 37 $^{\circ}\text{C}$ and 5% CO_2 .^{21,22}

The ability of PNCE to target *in vitro*

We first extracted MOMCs and tumor membranes. Next, the membranes containing CXCR 4 were enveloped on 96-well plates overnight. Then, the DiI labeled released PNCE (PNCE-DiI) were incubated with cellular membranes for 2 h. Then, the plates were washed 3 times by using buffer solution. The fluorescence intensity was determined using Molecular Devices ID 5 (Silicon Valley, USA).

The sensitive release ability of PNCE from CXCR 4 by MMP-2 *in vitro*

MMP-2 (2 $\mu\text{g mL}^{-1}$, 100 μL) was incubated with MOMCs@PNCE-DiI for 4 h. Then the plates were washed 3 times by using buffer solution. And the fluorescence intensity was detected by Molecular Devices ID 5.

The affinity of PNCE and MOMCs *in vitro*

The MOMCs were seeded in a 35 mm glass bottom dish overnight (2×10^4 cells per dish). The cells were incubated with PNCE-DiI for 30 min, 1 h, 2 h and 4 h. After washing 3 times with buffer solution, the MOMCs were incubated with DiO (10 μM) for 30 min at 37 $^{\circ}\text{C}$. Then, the nucleus was marked with DAPI for 30 min (1 μM). And then the fluorescence intensity of coumarin-6 (C6) was detected by confocal laser scanning microscopy (CLSM).

The ability of PNCE to target MOMCs *in vitro*

The MOMCs were seeded in a 6-well plate overnight (2×10^5 cells per dish). The cells were incubated with PNCE for 2 h. After that, the particle size and zeta potential were detected using NanoBrook Omni (New York, USA).

The sensitive release ability of PNCE from MOMCs

The MOMCs were seeded in a 6-well plate overnight (2×10^5 cells per dish). The cells were incubated with PNCE for 2 h. After that, MMP-2 (2 $\mu\text{g mL}^{-1}$, 1 mL) was added into the wells for 1 h at 37 $^{\circ}\text{C}$, and then the particle size and zeta potential were detected using NanoBrook Omni (New York, USA).

Cellular uptake efficiency

The fibroblasts and macrophages were seeded in a 35 mm glass bottom dish overnight (2×10^4 cells per dish). And then the cells were incubated with C6 labeled released PNCE (PNCE-C6) and free C6 (10 $\mu\text{g mL}^{-1}$ of C6 concentration) in RPMI-1640 with free FBS for 1 h and 4 h. The fluorescence intensity of C6 was detected by confocal CLSM.

Lysosomal escape efficiency of PNCE-C6

The fibroblasts and macrophages were cultured in a 35 mm glass bottom dish overnight (2×10^4 cells per dish). The cells were incubated with released PNCE-C6 (10 $\mu\text{g mL}^{-1}$ of C6 concentration) for 30 min and 4 h, and then washed 3 times with PBS. Then the lung fibroblasts and macrophages were fixed with 4% paraformaldehyde, respectively. And the lysosomes were marked using the LysoTracker Red DND-99 kit (50 nM). Lung fibroblasts were examined by CLSM.

Cytotoxicity

The cytotoxicity of PNCE was evaluated in macrophages and lung fibroblasts *via* a standard MTT assay. The macrophages and lung fibroblasts were seeded in a 96-well plate (5×10^4 and 2×10^4 cells per well) for 24 h. The macrophages and fibroblasts were incubated with LPS (2 $\mu\text{g mL}^{-1}$) and TGF- β (5 ng mL^{-1}) for 24 h, respectively. And then the cells were treated with different concentrations of PNCE, PNC, PN and PC at 37 $^{\circ}\text{C}$ under 5% CO_2 . The cells were utilized as normal cells with non-treatment. MTT solution (20 μL , 5 mg mL^{-1}) was added into wells incubated for 4 h. Then media were removed carefully, and 200 μL DMSO solution was added into wells. The absorbance was measured with a microplate reader at 490 nm, and then the cell viability was examined.

Content of TGF- β and IL-1 β *in vitro*

The macrophages were respectively seeded in 96-well plates (5×10^4 cells per well) for 24 h. The macrophages and fibroblasts were incubated with LPS (2 $\mu\text{g mL}^{-1}$) and TGF- β (5 ng mL^{-1}) for 24 h, respectively. After that, the cells were treated with PNCE, PNC, PN and PC (400 ng mL^{-1} NIN and 400 ng mL^{-1} COL in each group) at 37 $^{\circ}\text{C}$ under 5% CO_2 . 10 μL of the media was removed to detect the content of TGF- β and IL-1 β by enzyme linked immunosorbent assay (ELISA) at 4 h, 12 h, and 24 h.

Immunofluorescence staining of α -SMA and collagen I

The fibroblasts were cultured in 6-well plates with a cell climbing slice (2×10^5 cells per well) for 24 h. The cells were incubated with PNCE, PNC, and PN (400 ng mL^{-1} NIN in each formulation) in RPMI-1640 with TGF- β (5 ng mL^{-1}) media for 24 h. The media were removed and the cell climbing slices were washed with PBS 3 times, and then the cell climbing slices were fixed with 4% paraformaldehyde. The expressions of α -SMA and collagen I were evaluated *via* immunofluorescence staining.

The expression of α -SMA and CD 68 in a co-culture model

The therapeutic efficacy was determined to evaluate the myofibroblast and M1 macrophage differentiation after treating with different formulations using the transwell devices. Firstly, we investigated the myofibroblast transformation. The macrophages were cultured into upper chambers with pore sizes of 8.0 μm at 2×10^4 cells per well in 100 μL of FBS-free RPMI-1640 media and then inserted in a 24-well plate. Subsequently, the fibroblasts (5×10^4) were seeded into lower chambers with 24-well climbing slices in 600 μL of RPMI 1640 media with 10% FBS. Then, various formulations (400 ng mL^{-1} NIN in each group) were added into upper and lower chambers and incubated for 24 h. And next, we utilized immunofluorescence staining to measure the expression of α -SMA. Secondly, we detected the expression of CD 68 which was a pro-inflammatory marker in macrophages. The fibroblasts were cultured into upper chambers with a pore size of 8.0 μm at 2×10^4 cells per well in 100 μL of FBS-free RPMI-1640 media and then inserted in a 24-well plate. Subsequently, the macrophages (5×10^4) were seeded into lower chambers with 24-well climbing slices in 600 μL of RPMI 1640 media with 10% FBS.

Wound-healing assay

The fibroblasts or macrophages were seeded into a 6-well plate with 3×10^5 cells per dish, and then incubated for 24 h. After that, the cells were spread over the dish entirely, the scarification was done with a 10 μL pipette device in the middle of the dish, and the floating cells were removed with PBS. Then, different formulations of PN, PNC and PNCE (400 ng mL^{-1} NIN in each formulation) containing TGF- β (5 ng mL^{-1}) or LPS (2 $\mu\text{g mL}^{-1}$) were incubated with the fibroblasts or macrophages for 24 h, respectively. The extents of wound healing were observed using an inverted microscope in each group.

Expression of monocyte chemo-attractant protein-1 (MCP-1) in macrophages and platelet derived growth factor (PDGF) in fibroblasts

For the expression of MCP-1 or PDGF, macrophages or fibroblasts were cultured in 6-well plates with cell climbing slices (2×10^5 cells per well) for 24 h. The cells were treated in RPMI-1640 and free FBS with LPS (2 $\mu\text{g mL}^{-1}$) or TGF- β (5 ng mL^{-1}) media for 24 h, and then the cells were incubated with PNCE, PNC, and PN (400 ng mL^{-1} NIN in each treatment) in RPMI-1640 with LPS (2 $\mu\text{g mL}^{-1}$) or TGF- β (5 ng mL^{-1}) media for 24 h. The climbing slices of macrophages and fibroblasts were fixed with 4% paraformaldehyde. The cell climbing slices were incubated with primary antibodies of mouse anti-MCP-1 or mouse anti-PDGF which was diluted with 1:1500 and 1:1000, respectively. Then cell climbing slices were washed with PBS solution 3 times and incubated with the secondary antibody of fluorescent tagged goat anti-mouse IgG (1:1000 dilution) for 1 hour. Finally, the expressions of MCP-1 and PDGF were evaluated using an immunofluorescence microscope.

The content of ROS

For the content of ROS, fibroblasts were cultured into a 24-well plate with 5×10^4 cells per well for 24 h. The cells were stimulated in RPMI-1640 and free FBS with TGF- β (5 ng mL^{-1}) media for 24 h firstly, then the cells were treated with PNCE, PNC, and PN (400 ng mL^{-1} NIN in each formulation) in RPMI-1640 and free FBS with TGF- β (5 ng mL^{-1}) media for 24 h. The media were removed, and DCFH-DA (5 μM) was added and incubated in RPMI-1640 with free FBS media in the dark for 15 min. Then the cells were imaged with an inverted fluorescence microscope.

Biodistribution of DiR labeled-PNCE (PNCE-DiR) and DiR labeled-PNC (PNC-DiR)

IPF mice (21 days after injection of BLM) were evaluated for biodistribution of PNCE-DiR, PNC-DiR and DiR. Then PNCE-DiR, PNC-DiR and DiR were administrated by intravenous injection. We first monitored the biodistribution of the PNCE-DiR, PNC-DiR after intravenous injection using an *in vivo* imaging system (Image Station *In Vivo* FX, USA). We further examined the quantity of DiR in the major organs, including the lung, heart, liver, spleen and kidneys to assess the distribution of PNCE-DiR, PNC-DiR and DiR, shown as the mean fluorescence intensity in the region of interest (ROI).

Target ability to MOMCs of PNCE-DiI

IPF mice were administrated PNCE-DiI and PNC labeled DiI (PNC-DiI) to evaluate the target ability. After sacrifice of mice at 2 h after intravenous injection, the lungs were obtained and fixed with 4% paraformaldehyde. Then the lung sections were deparaffinized and blocked for 30 min. The MOMCs were labeled with the primary antibodies of CD 45, CXC chemokine receptor-7 (CCR 7) and CD 11b of green, which were diluted with 1:1000, 1:500 and 1:500, respectively. The lung tissues were incubated with primary antibodies overnight at 4 $^{\circ}\text{C}$. Then lung slides were incubated with the secondary antibody of goat anti-mouse and goat anti-rabbit IgG (1:1000 dilution), respectively, for 1 h. Then lung sections were observed under a fluorescence microscope.

Sensitive release ability of PNCE from MOMCs

IPF mice were administrated PNCE-DiI to evaluate the sensitive release ability. After sacrifice of mice at different time points (30 min, 2 h) after intravenous injection the lungs were obtained and fixed with 4% paraformaldehyde. Then the lung sections were deparaffinized and blocked for 30 min. The MOMCs were labeled with the primary antibodies of nanog of green, which were diluted with 1:200. The lung tissues were incubated with primary antibodies overnight at 4 $^{\circ}\text{C}$. Then lung slides were incubated with the secondary antibody of goat anti-mouse IgG (1:1000 dilution) for 1 h. Then lung sections were observed under a fluorescence microscope.

Biodistribution of PNCE-DiI in macrophages and fibroblasts

IPF mice were administrated with PNCE-DiI to investigate the accumulation in macrophages and fibroblasts. After the sacrifice of mice at 4 h after intravenous injection, the lungs were obtained and fixed with 4% paraformaldehyde. Then the lung sections were deparaffinized and blocked for 30 min. The macrophages and fibroblasts were labeled with the primary antibodies of F4/80 and CD 90 diluted with 1 : 1000 and 1 : 800 of green, respectively. Then lung slides were incubated with the secondary antibody of goat anti-mouse and goat anti-rabbit IgG (1 : 1000 dilution) for 1 h. Then lung sections were observed under a fluorescence microscope.

Anti-fibrosis efficiency of PNCE, PNC and PN *in vivo*

IPF mice were randomly divided into five groups with five mice per group: (1) BLM, (2) normal, (3) PN, (4) PNC and (5) PNCE. To evaluate the treatment efficacy of PNCE, PNC and PN, IPF mice were treated with PNCE, PNC and PN by intravenous administration. The solution of drugs (100 μ L, containing 0.6 mg mL⁻¹ of NIN or 0.12 mg mL⁻¹ of COL) was administered by intravenous injection. Mice were administrated drugs at day 2, 4, and 6 by intravenous injection. All the animals were sacrificed on day 21, and lungs were fixed or frozen for further analysis.

TGF- β and IL-1 β content by ELISA analysis

IPF progress could be accelerated by the innate immune system, which led to the excessive proliferation of TGF- β and IL-1 β .²³ The frozen lung tissues were homogenized for further analysis of inflammation concentration. The contents of TGF- β and IL-1 β were detected by ELISA assay. The absorbance was measured at 450 nm by UV-vis analysis.

Lung histology

IPF mice (21 days after treatment with PNCE, PNC and PN) were anesthetized and sacrificed. The harvested lung tissues were fixed in 4% paraformaldehyde solution, and then embedded and sectioned in paraffin. Lung sections were then subjected to hematoxylin and eosin staining (H&E staining) and Masson staining. Then lung sections were observed under a light microscope. H&E staining and Masson trichrome were used to evaluate the degree of lung injury and collagen deposition in lung tissues, respectively.

Immunohistochemistry (IHC)

The expressions of α -SMA and collagen I in lung tissues were evaluated by IHC. The lung sections were deparaffinized and blocked for 30 min. Then primary antibodies of mouse anti- α -SMA and mouse anti-collagen I were diluted to 1 : 1000 and 1 : 500, respectively. The slides were incubated with primary antibodies overnight at 4 °C. Then lung slides were washed with PBS solution 3 times and incubated with the secondary antibody of goat anti-mouse IgG (1 : 1000 dilution) for 1 h. Then lung sections were observed under a light microscope. Furthermore, we also detected the proportion of

M2 macrophages in lungs. The lung sections were incubated with the primary antibodies of mouse anti-CD 163 (1 : 500) and mouse anti-CD 68 (1 : 800) overnight at 4 °C. Then lung slides were washed with PBS solution 3 times and incubated with the secondary antibody of goat anti-mouse IgG (1 : 1000 dilution) for 1 h. Then lung sections were observed under a fluorescence microscope.

Serum biochemistry analysis

The whole blood samples for biochemical detection were collected in an Eppendorf stand for 2 h at room temperature, and then centrifuged at 3500 rpm for 10 min at 4 °C to gain the serum samples. We further analyzed alanine aminotransferase (ALT), aspartate aminotransferase (AST) and blood urea nitrogen (BUN) using an automated analyzer.

Inflammatory cell analysis in whole blood

The whole blood was obtained from the eye orbit of mice and stored in an anticoagulant tube containing EDTA. White cells, lymphocytes, monocytes and neutrophils were detected using a blood analyzer (Premier 3000, USA).

Statistical analysis

Data were calculated and processed as standard error of measurement (mean \pm S.E.M.). Comparison between all the groups was performed with one-way analysis of variance (ANOVA), and the data between two groups were determined with Student's *t*-test. Statistical significance was defined as **P* < 0.05, ***P* < 0.01. ****P* < 0.001.

3. Results and discussion

Preparation and characterization of PNCE

PNCE liposomes were prepared by the film dispersion method.²⁴ The dual drugs NIN and COL could be encapsulated into the hydrophobic layer and hydrophilic layer of the vehicle by hydration, respectively (Fig. 1A). The peptide E5 was grafted into the PNCE by Michael reaction. As determined by sodium dodecyl sulfate–polyacrylamide gel electrophoresis (SDS-PAGE) (Fig. 1B), ¹H NMR spectroscopy (Fig. S1†) and infrared spectroscopy (Fig. S2†), we successfully prepared PNCE and the grafting rate of peptide E5 in the PNCE was 57.9%. The particle size of PNCE was 99.88 \pm 4.15 nm, as determined by dynamic light scattering (DLS) (Fig. 1C), and PNCE showed a homogeneous morphology of spherical nanoparticles by transmission electron microscopy (TEM). The PC, PN and PNC were prepared as control treatment groups, and the relative particle sizes were 91.45 \pm 5.69 nm, 91.11 \pm 6.14 nm and 106.16 \pm 7.49 nm, respectively (Table S1†). The absorbance of NIN at 391 nm and that of COL at 350 nm were observed by UV-vis spectroscopy with PNCE, which indicated that both drugs were encapsulated into the hydrophilic and hydrophobic layers of PNCE (Fig. 1D). Considering that there is some overlap between NIN and COL absorption at 350 nm, the drug contents of NIN and COL in the liposomes were determined by

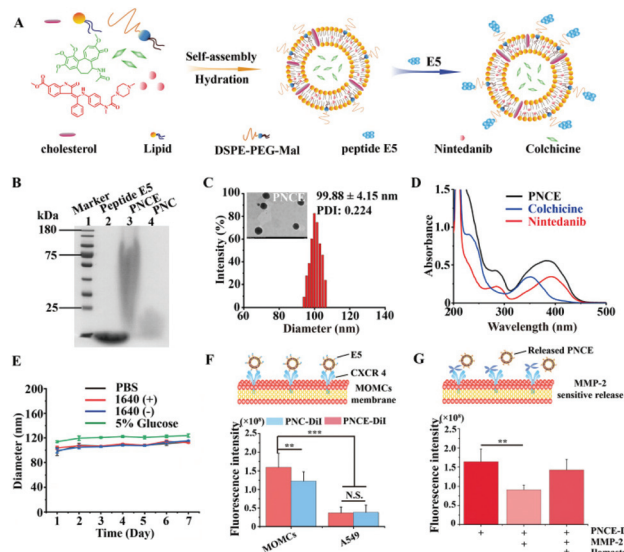


Fig. 1 PNCE design, preparation, and characterization. (A) Schematic showing the preparation of PNCE. (B) The SDS-PAGE of peptide E5, PNCE and PNC. (C) The size distribution and TEM images of the PNCE. (D) UV-vis absorption spectra of the NIN, COL, and PNCE. (E) The stability test of PNCE under the conditions of PBS, 1640 (+) and 5% glucose. (F) The targeting ability of peptide E5 to CXCR 4 ($n = 9$). (G) The sensitive release ability of PNCE from MOMCs by MMP-2 ($n = 9$).

RP-HPLC, respectively (Fig. S3 and S4[†]). The EE % of NIN in PNCE was $105.84 \pm 8.37\%$, and the EE % of COL was $68.91 \pm 7.61\%$. The LE % of NIN in PNCE was $1.34 \pm 0.02\%$, and the LE % of COL was $3.45 \pm 0.07\%$ (Table S2[†]). As shown in Fig. 1E, PNCE showed good stability in the media of PBS, RPMI 1640 (+) and 5% glucose, implying that the PNCE was a long circulating liposome, which is beneficial for treating disease. Moreover, we investigated the targeting ability of PNCE to CXCR 4 *in vitro*.^{25–27} The A549 membrane protein was chosen as the control group, which barely expressed the CXCR 4 receptor. The results showed that the fluorescence intensity in the MOMC group increased 2-fold compared to that in the A549 group. In addition, compared with DiI labeled PNC-DiI, PNCE-DiI had a stronger fluorescence intensity. The data indicated that the MOMC membrane protein could specifically conjugate with PNCE-DiI (Fig. 1F). In addition, most of the PNCE would bind to CXCR 4 on MOMCs and not be internalized within a certain time. The main reason was that functional CXCR 4 was overexpressed and mediated cell migration rather than endocytosis.^{28–30} Furthermore, the sensitive release ability of PNCE from MOMCs was detected *in vitro*. The results demonstrated that PNCE was separated from the MOMCs after incubating with MMP-2, confirming that PNCE could be released sensitively from MOMCs by MMP-2. However, this result disappeared after incubation of ilomastat with MOMCs@PNCE (Fig. 1G). The main reason is that ilomastat is an antagonist of MMP-2, which can inhibit the activity of MMP-2 without releasing PNCE-DiI.

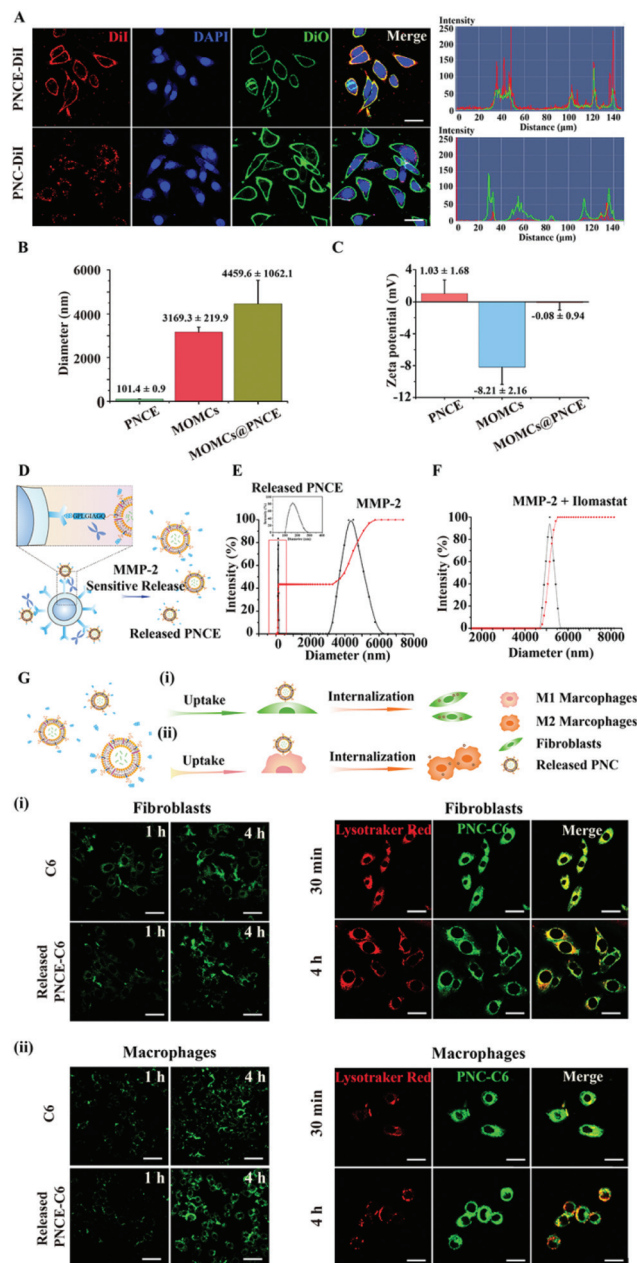


Fig. 2 Specific recognition, sensitive release, cellular uptake and intracellular localization *in vitro*. (A) Characterization of the interaction of MOMCs with DiI labeled PNC and PNCE. (B) The particle size of PNCE, MOMCs and MOMCs@PNCE. (C) The zeta potential of PNCE, MOMCs and MOMCs@PNCE. (D) Schematic of MMP-2-mediated sensitive release of PNCE from MOMCs. (E) The changes of particle size in MOMCs@PNCE after incubating with MMP-2. (F) The changes of particle size in MOMCs@PNCE after incubating with MMP-2 and ilomastat (MMP-2 inhibitor). (G) Schematic of the uptake and internalization of the released PNCE-coumarin 6; (i) cellular uptake and lysosome escape analyzed by CLSM in fibroblasts; (ii) cellular uptake and lysosome escape analyzed by CLSM in macrophages. Scale bars: 40 μm .

Specific recognition, sensitive release, cellular uptake and intracellular localization *in vitro*

The prerequisites for PNCE to be able to treat IPF *in vivo* are their effective adhesion to the MOMCs. To explore the efficient

targeting ability of PNCE for MOMCs *in vitro*, the specific adhesion of PNCE to MOMCs was investigated. The MOMCs were isolated from the peripheral blood of IPF mice according to a reported method.^{21,22} The morphologies of MOMCs were fusiform, and similar to stem cells. First, MOMCs were incubated with PNC-DiI and PNCE-DiI and imaged by CLSM (Fig. 2A). The confocal images showed that PNCE-DiI exhibited a stronger red fluorescence on the surface of MOMCs rather than in the cytoplasm. The results implied that PNCE had a good affinity for MOMCs at different times, which was necessary for the effective treatment of IPF (Fig. S5†). In addition, we also measured the particle size and zeta potential of MOMCs@PNCE. The data demonstrated that the particle sizes of MOMCs@PNCE increased and the zeta potential also changed, which indicated that PNCE could conjugate to MOMCs (Fig. 2B and C). Furthermore, the PNCE would be released in the form of MOMCs@PNCE due to the inclusion called GPLGIAGQ in E5 which could be cut by MMP-2³¹ over-expressed in IPF lungs (Fig. 2D–F). Then, the detached PNCE would be distributed to the IPF lungs, taken up and internalized by macrophages and fibroblasts, respectively (Fig. 2G). Moreover, the intracellular behavior of drugs affected the therapeutic effect of PNCE. The results suggested that fibroblast uptake was a time dependent manner, and the uptake of the released PNCE-C6 was similar to that of C6. Then, the localization of the released PNCE-C6 and lysosomal escape in

lung fibroblasts were carried out by CLSM. The green fluorescence of the released PNCE-C6 overlapped completely with the red fluorescence from the lysosomes stained with LysoTracker in 30 min, which implied that the released PNCE-C6 was taken up into cells and then accumulated in lysosomes. Then, the green fluorescence mainly increased in the cytoplasm and separated from the red fluorescence after 4 h, which indicated that the released PNCE-C6 could escape from lysosomes in a time-dependent manner. Then the cellular uptake and intracellular localization in macrophages were also investigated by CLSM, which showed that the released PNCE-C6 could be taken up by macrophages and escape from lysosomes.

Treatment efficacy of PN, PNC and PNCE *in vitro*

To investigate the anti-fibrosis effect of PNCE, PNC and PN, we firstly evaluated their effective concentration in primary macrophages and lung fibroblasts to determine the secure dosing range assessing the toxicity *in vitro*. At concentrations of NIN less than 400 ng mL⁻¹, the cell viabilities of macrophages and fibroblasts were not influenced and the survival rates of those were more than 80% (Fig. 3A and B). Thus, we chose this dose as the desired concentration for further study. Interestingly, compared with PN, PNCE and PNC showed significant cytotoxicity at concentrations of NIN more than 3.2 μg mL⁻¹ in macrophages, likely because COL could collaborate with NIN

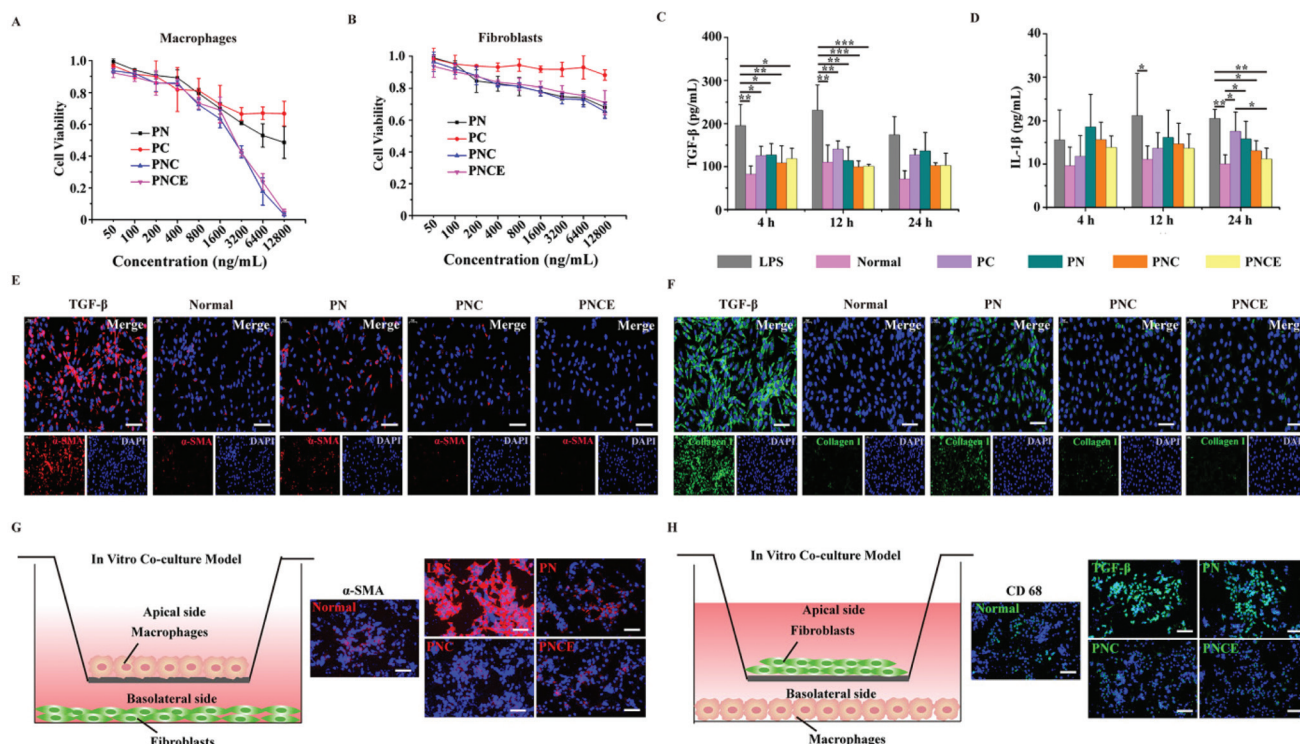


Fig. 3 Anti-fibrosis effect of PNCE and PNC *in vitro*. (A) Cytotoxicity of primary macrophages after treating for 24 h with PN, PNC and PNCE. (B) Cytotoxicity of primary fibroblasts after treating for 24 h with PN, PNC and PNCE ($n = 3$). (C, D) The levels of TGF- β (C) and IL-1 β (D) after treating with PN, PNC and PNCE in primary macrophages ($n = 3$). (E) Immunofluorescence staining for α -SMA (red) after treating for 24 h. Scale bar: 100 μ m. (F) Immunofluorescence staining for collagen I (green) after treating for 24 h. Scale bar: 100 μ m. (G, H) Anti-fibrosis effect of PNCE and PNC in a co-incubation model. Scale bar: 100 μ m.

to inhibit the proliferation of macrophages.¹⁶ This result was powerful for predicting the subsequent anti-fibrosis effect *in vivo*, because macrophages show over-proliferation during the progression of IPF. Besides, the proliferation of fibroblasts was also inhibited with the PNCE and PNC compared to PN at the concentration of 400 ng mL⁻¹ of NIN.

To further demonstrate the hypothesis that COL combined with NIN could reduce cytokine secretion in macrophages, we evaluated the content of IL-1 β and TGF- β *in vitro*. We confirmed the inhibitory efficiency of PNCE, PNC and PN by assessing the content of IL-1 β and TGF- β in macrophages using the ELISA assay. After treating with LPS, the level of TGF- β was significantly improved compared to the normal group. After stimulating for 24 h, the macrophages were incubated with PNCE, PNC and PN to evaluate the content of IL-1 β and TGF- β (Fig. 3C and D). The PNCE and PNC had significantly powerful capacities to reduce the inflammatory factor expression. The reducing levels of TGF- β and IL-1 β contents in the PNCE and PNC groups increased 1-fold and 0.5-fold compared with that in PN, respectively. We further evaluated the anti-fibrotic efficacy of PNCE, PNC and PN *via* detecting α -SMA and collagen I expression *in vitro*, which were the crucial indicators to predict myofibroblast activation.²³ The expressions of α -SMA and collagen I were detected *via* immunofluorescence staining after incubating with PNCE, PNC and PN for 24 h in IPF fibroblasts (Fig. 3E and F). The expression of α -SMA and collagen I had significantly decreased after treating with PNCE and PNC compared with that after treating with PN in fibroblasts, which demonstrated that NIN collaborated with COL had an effective capability to treat IPF *in vitro*. Then, the anti-fibrosis effect was also investigated during the co-incubation of macrophages and fibroblasts. The expressions of α -SMA in fibroblasts and CD 68 in M1 macrophages were reduced in the PNCE and PNC

groups, which also demonstrated that the PNCE and PNC could inhibit fibroblast activation and M1 macrophage proliferation by the synergistic effect of COL and NIN (Fig. 3G and H).

Treatment mechanism of PNCE *in vitro*

The main reason for the anti-fibrosis effect of NIN is that M1 macrophages secrete quantities of inflammatory factors, such as IL-1 β to promote the re-activation of fibroblasts (Fig. 4A). In the early IPF, the macrophages are mainly M1 macrophages to promote the inflammatory activation and accelerate the IPF progression. If the proportion of M1 to M2 is balanced after treating with formulations, the development of IPF will be shut down, achieving better anti-fibrosis effects. And then we calculated the proportion of M1 and M2 macrophages after treating with different formulations by immunofluorescence staining. It was observed that the quantity of M1 macrophages increased significantly compared to normal after stimulated by LPS, and the proportion of M1 and M2 was close to equilibrium after PNCE and PNC treatment (Fig. 4B). Furthermore, we also examined the expression of NF- κ B and ERK 1/2, which were the key pathways for macrophage polarization. The results showed that PNCE could effectively reduce the expressions of NF- κ B and ERK 1/2, and promote the proliferation of M2 macrophages, which was beneficial for enhancing the IPF therapy (Fig. 4C). Therefore, it was a prerequisite for effective treatment of IPF to regulate innate immune response before or simultaneously inhibiting fibroblast activation. In addition, the migration of macrophages and fibroblasts could also aggravate the progress of IPF.^{32,33} In the wound healing experiment (Fig. 4D), the PNCE and PNC groups could inhibit the invasion ability of primary fibroblasts, and about 250 μ m and 225 μ m were shortened compared with

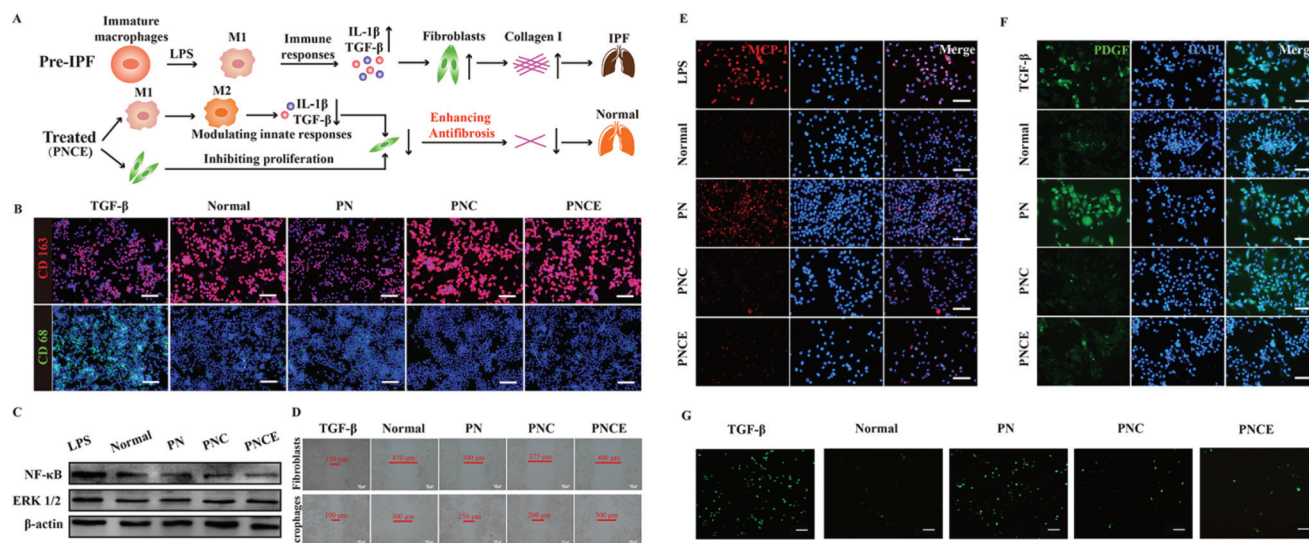


Fig. 4 Anti-fibrosis mechanism of PNCE and PNC *in vitro*. (A) Schematic of the progression and treatment of IPF. (B) The proportion of M1 and M2 macrophages. Scale bar: 200 μ m. (C) The expression of NF- κ B and ERK 1/2. (D) Wound-healing assay of primary fibroblasts and macrophages, respectively. Scale bar: 100 μ m. (E) The level of MCP-1 in LPS induced macrophages. Scale bar: 100 μ m. (F) The level of PDGF in TGF- β induced fibroblasts. Scale bar: 100 μ m. (G) The content of ROS in TGF- β induced fibroblasts after incubating with different formulations. Scale bar: 100 μ m.

the TGF- β induced fibroblasts, respectively. In the PN group, the wound healing capacity of cells was also inhibited to some extent; the wound healing was shortened to about 150 μm compared to TGF- β induced fibroblasts, indicating that the combination of NIN and COL had a synergy effect to inhibit fibroblast proliferation and differentiation compared to single NIN. Furthermore, we also detected the capacity of inhibiting macrophages in various formulations. The shortened distance in PNCE, PNC and PN was 200 μm , 100 μm and 50 μm , respectively. The results implied that the PNCE group had the strongest ability to inhibit cell invasion compared to PNC and PN groups. MCP-1 was a small cytokine in the CC chemokine, which played an important role in the pro-inflammatory chemotactic activation effect on macrophages. The images of the MCP-1 level showed that the expression was obviously decreased in the PNCE and PNC groups, and the efficacy of the PNCE group was better than that of the PNC group (Fig. 4E). The combination of COL and NIN could inhibit the secretion of inflammatory cytokines by macrophages, and the inflammatory response was also blocked in IPF. We further investigated the expression of PDGF in fibroblasts, which was an indicator to evaluate the activation of fibroblasts transforming into myofibroblasts. The PDGF expression was significantly reduced in the PNCE group, and PNC could also inhibit the expression of PDGF. However, PN showed the worst ability for PDGF inhibition (Fig. 4F); this demonstrated that dual-drug combination could effectively inhibit the activation of fibroblasts and thus decrease the accumulation of the ECM to achieve the treatment of IPF. The activation of fibroblasts may be due to oxidative stress.³⁴ The content of ROS in fibroblasts was also investigated by DCFH-DA (Fig. 4G). The results displayed that the extensive increase of ROS content could be alleviated to some extent after treating with PNCE compared with the control groups, which suggested that PNCE could inhibit the activation of fibroblasts to myofibroblasts by regulating oxidative stress.

Biodistribution of PNCE and PNC

The biodistribution of the DiR labeled PNCE and PNC was then investigated using an *in vivo* living system. Detection of accumulation of DiR labeled PNCE and PNC in the lungs was performed using IPF mice at 1, 8, and 24 h after intravenous injection. The DiR fluorescence in the PNCE-DiR group was found to accumulate mainly in the lungs compared with that in PNC-DiR (Fig. 5A). In addition, the lung fluorescence intensity achieved the highest level at 8 h in the PNCE-DiR group, and the fluorescence was still detected at 24 h; however, there was almost no fluorescence in the lungs of the PNC-DiR group. The result suggested that PNCE-DiR could accumulate efficiently in the lungs depending on the MOMC homing ability compared to the PNC-DiR group. To accurately analyze the fluorescence, we further measured it in the major organs, including the lungs and other organs (liver, heart, spleen and kidneys) at the time points mentioned above. The trend of fluorescence intensity in the lungs was the same as that in

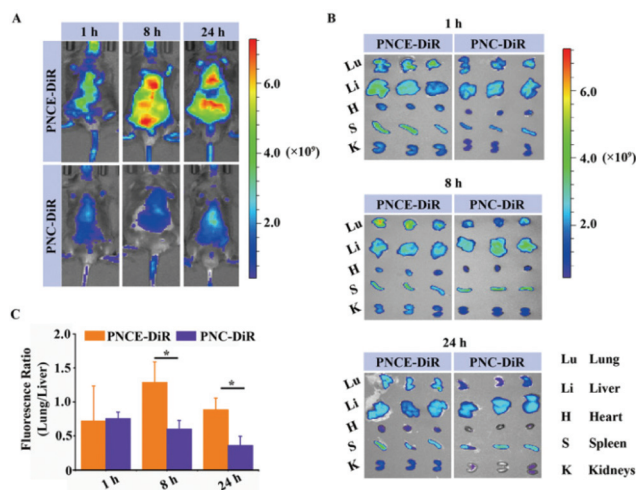


Fig. 5 Biodistribution of the PNCE-DiR and PNC-DiR after intravenous injection. (A) *In vivo* fluorescence images of BLM-induced IPF mice obtained at 1 h, 8 h and 24 h post-injection with PNCE-DiR and PNC-DiR. (B) *Ex vivo* fluorescence images of the lungs, heart, liver, spleen and kidneys at 1 h, 8 h and 24 h post-injection. (C) Quantitative analysis of the *ex vivo* DiR fluorescence intensity of the lung/liver at different point times ($n = 3$).

in vivo imaging (Fig. 5B). A stronger fluorescence was observed in the lungs and little was found in the liver. These results indicated that PNCE-DiR could effectively deliver drugs to the lungs depending on the targeted ability of peptide E5 to circulating MOMCs, which were recruited to the lungs *via* receptors and the ligand *in vivo*. Furthermore, we also evaluated the fluorescence intensity of DiR at different time points in the PNCE-DiR and PNC-DiR groups (Fig. 5C). The fluorescence accumulated the most in the lungs at 8 h in the PNCE-DiR group. By contrast, there was little fluorescence in the lungs in the PNC-DiR group. Moreover, the PNCE-DiR group still had accumulated fluorescence in the lungs at 24 h, which showed that PNCE-DiR had a long period of systemic circulation and it was beneficial for the long-term treatment of IPF *in vivo*.

Target mechanism of PNCE-DiI to MOMCs

To confirm our hypothesis, we evaluated the mechanism of PNCE-DiI accumulated efficiently in the lungs depending on the MOMC homing capacity by tracer experiment. DiI acted as a tracer to present PNCE-DiI behavior, and Nanog expressed by MOMCs was labeled with green fluorescence. The fluorescence intensity of DiI in the IPF lungs is shown in Fig. 6A after administration of PNCE-DiI and PNC-DiI *via* intravenous injection. The DiI fluorescence of PNCE-DiI had higher fluorescence intensity in the lungs than that in the PNC-DiI group. Meanwhile, the green fluorescence and red fluorescence overlapped completely, which may be due to the fact that PNCE-DiI adhered to MOMCs firstly in the circulation and then was delivered to the lungs. Then, we further labeled CCR-7 in green, which was overexpressed on the surface of

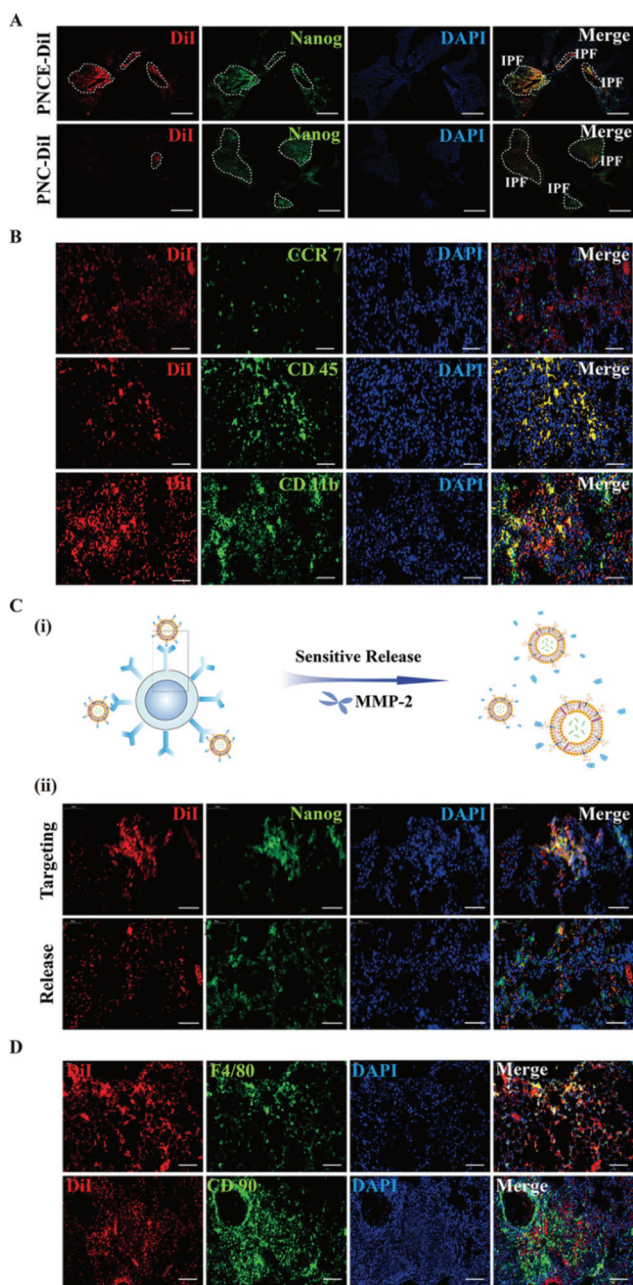


Fig. 6 The targeting mechanism of PNCE-DiI to IPF lung tissues after intravenous injection. (A) The targeting ability of PNCE-DiI and PNC-DiI to IPF lung tissues *in vivo*. Scale bars: 2 mm. (B) Representative fluorescence intensity showing CCR-7, CD45 and CD11b labeled MOMCs (green) and treated with PNCE-DiI in lung tissues. (C) Schematic showing the sensitive release process of PNCE from MOMCs and the process of released PNCE-DiI from MOMCs. Scale bars: 50 μm . (D) Biodistribution of PNCE-DiI in macrophages and fibroblasts. Scale bars: 100 μm .

MOMCs. The fluorescence intensity was observed in lung sections and a large amount of red fluorescence appeared around the green fluorescence. The results implied that PNCE-DiI could follow MOMCs exactly to the lungs due to the homing

ability of MOMCs. In addition, it is possible that some of the PNCE may not be delivered to the lungs due to the complexity of systemic circulation *in vivo*, and PNCE of this part may have been delivered to other organs or cleared. Then, we verified the targeting ability of PNCE-DiI by two antibodies of leukocyte common antigen (CD 45 and CD 11b) (Fig. 6B). The results of fluorescence intensity indicated that PNCE-DiI overlapped with MOMCs labeled with green fluorescence, showing a yellow fluorescence. The result ensured that PNCE-DiI could target MOMCs *in vivo* and then be delivered to the lungs due to the homing ability of MOMCs. This situation demonstrated that PNCE could be delivered to the lung tissues and confirmed the therapeutic efficacy for IPF. This strategy of efficient drug delivery provided the basis for better treatment of IPF. We further evaluated the sensitive separation of PNCE-DiI from the MOMC surface when MMP-2 overexpressed in the IPF lungs by immunofluorescence staining. The red fluorescence of DiI overlapped with the green signal of Nanog representing MOMCs after injecting PNCE-DiI for 30 min (Fig. 6C). And then the lungs were collected after administration for 2 h; the result showed that the red signal and the green signal were separated, which indicated that PNCE-DiI could be released from MOMCs to treat IPF. In addition, we also detected the fluorescence intensity of Nanog-bound PNCE-DiI on MOMCs at different times (Fig. S6[†]). Furthermore, we also measured the PNCE-DiI accumulation in macrophages and fibroblasts, respectively. The results showed that PNCE-DiI could overlap with fibroblasts and macrophages labeled with green fluorescence, which indicated that PNCE could be delivered to these cells for IPF therapy (Fig. 6D).

Anti-fibrotic effects of PNCE *in vivo*

After investigating the ability of accumulation and retention of PNCE in the lungs, various anti-fibrotic formulations were then administered to IPF mice by intravenous injection (Fig. 7A). We first evaluated the anti-fibrotic efficacy *via* H&E staining (Fig. 7B). The necrotic regions were decreased in the PNCE group than in the PNC, PN and BLM groups. In the BLM group, the lungs exhibited severe deficiency of parenchyma, and the alveoli diameter became larger and alveolar walls became thicker than those of the normal group. Meanwhile, infiltration of inflammatory cells including macrophages was also observed in lung tissues. In addition, lung tissues in the PNCE group showed significantly ameliorated IPF progression with decreasing inflammatory cell infiltration and a recovering bronchiolar structure normally compared with those in the PNC and PN groups. In addition, the quantities of alveoli in the PNCE were increased 0.5-fold, compared with the BLM group, which implied that mice breathing achieved the greatest improvement in the PNCE group than other treatments. Then we demonstrated the collagen deposition *via* Masson staining (Fig. 7C). Compared with the BLM group, collagen deposition as shown in the blue area obviously decreased after treatment with PNCE compared with the BLM group. The treatment efficacy of PNCE in H&E staining and Masson staining

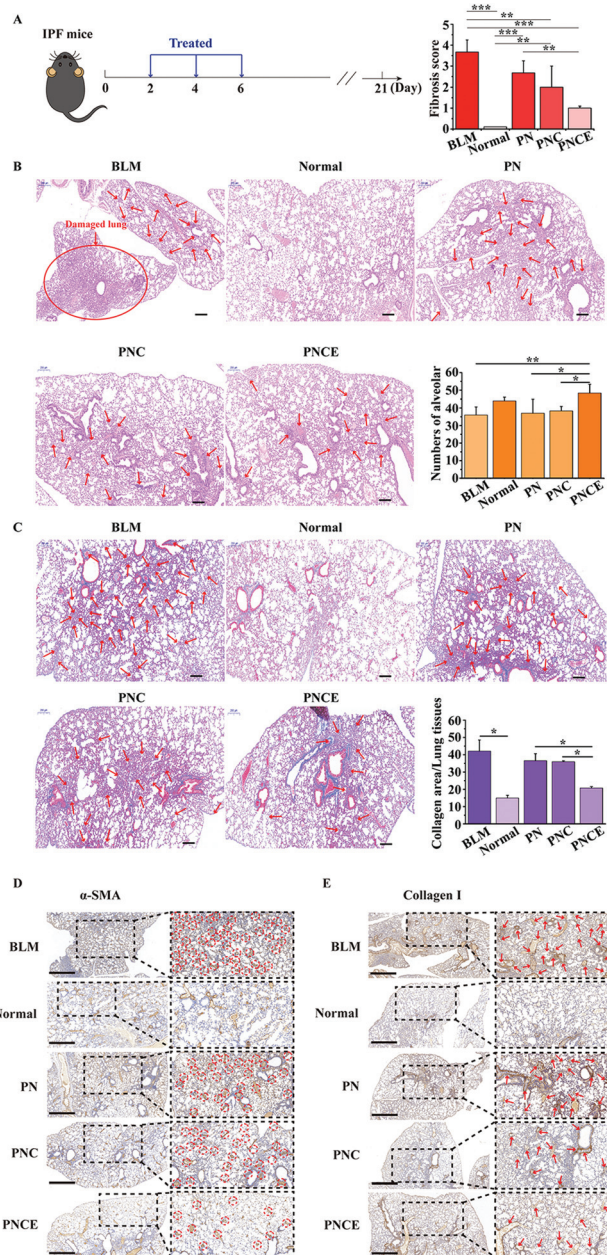


Fig. 7 Anti-fibrosis effects of PNCE, PNC and PN *in vivo* ($n = 5$). (A) Treatment scheme and fibrosis scores for IPF treatment. (B) H&E staining of lung tissues after different treatments. Scale bar: 200 μm . (C) Masson staining of lung tissues to evaluate collagen deposition after different treatments. Scale bar: 200 μm . (D) Representative IHC images of lung tissues stained with α -SMA. Scale bar: 1 mm. (E) Representative IHC images of lung tissues stained with collagen I. Scale bar: 1 mm.

was better than that of the PN and PNC groups. In addition, we confirmed the anti-fibrotic efficacy using IHC with α -SMA and collagen I. More decreasing expression of α -SMA was found in the PNCE group than in other groups (Fig. 7D). The expression of α -SMA was the crucial biomarker to evaluate the IPF treatment efficacy because it could determine whether

myofibroblasts were overactivated, and the data demonstrated that PNCE could inhibit myofibroblast over-activation effectively compared to other groups. The PNC had also a lower treatment efficacy than PN, however, it was not as effective as PNCE, owing to the lack of the lung-targeting ability. Similarly, the deposition of collagen I also decreased in the PNCE group; the decreasing trend was the same as α -SMA expression, indicating that the minimum area of collagen I deposition appeared in the PNCE group compared with other groups (Fig. 7E). Moreover, we also detected the biosecurity of different formulations by H&E staining. The results implied that the major organs were healthy after treatment for 21 days, demonstrating that systemic toxicity was rarely exhibited by intravenous injection of the PNCE, PNC and PN groups (Fig. S7A†). In addition, as shown in Fig. S7B–D,† there were no significant changes in the levels of AST, ALT and BUN, suggesting that the functions of the liver and spleen remained, and hepatocytes and nephrocytes were not damaged after administration with each group. These results indicated that the PNCE, PNC and PN groups rarely caused systemic toxicity after administration for IPF treatment.

Anti-fibrosis mechanism of PNCE *in vivo*

To further investigate the therapeutic mechanism of PNCE, we demonstrated the proliferation of inflammatory cells. With the

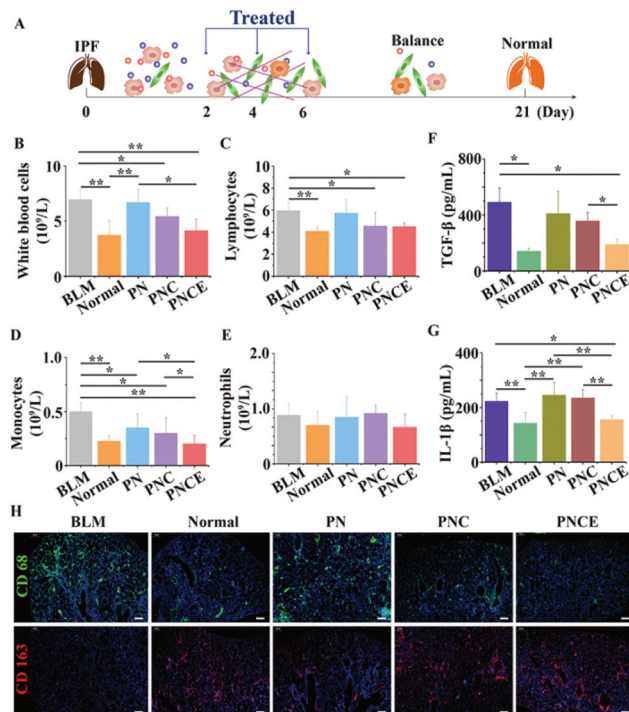


Fig. 8 Anti-fibrosis mechanism of PNCE *in vivo*. (A) Schematic of the anti-fibrosis mechanism of PNCE *in vivo*. (B) Proliferation of white blood cells. (C) Proliferation of lymphocytes. (D) Proliferation of monocyte cells. (E) Proliferation of neutrophil cells. (F) The level of TGF- β 1 in lung tissues. (G) The level of IL-1 β in lung tissues. The whole blood was tested in all groups ($n = 5$). (H) The expression of CD 163 and CD 68 after treating with different formulations. Scale bar: 200 μm .

progress of IPF, the proliferation of neutrophils and white cells is the main reason to induce lung parenchyma injury and fibrosis of the alveolar structure.³⁵ The schematic showed that PNCE treated IPF by regulating innate immune responses (Fig. 8A). Lower proliferations of white cells, lymphocytes, monocytes and neutrophils were observed in PNCE compared with other groups, suggesting that PNCE could inhibit the IPF process *via* blocking inflammatory response (Fig. 8B–E). Besides, we also detected the content of TGF- β and IL-1 β in lung tissues, which were the major cytokines in IPF that were involved in cell proliferation, differentiation, and ECM production.^{36,37} Furthermore, the expressions of TGF- β and IL-1 β in IPF lung tissues were significantly decreased expression in PNCE (Fig. 8F and G). Besides, the treatment efficacy of PNCE was better than that of the PNC and PN groups. The main reason for the poor therapeutic effect was the deficiency of a lung targeted or dual drug synergistic effect in the PNC and PN groups. In addition, we also detected the proportion of M1 macrophages after treating with different formulations (Fig. 8H). The population of M1 macrophages exhibited significant reduction in PNCE than in the PN and BLM groups, which suggested that the effect of NIN on IPF treatment could be enhanced by regulating the immune response. In addition, effective delivery of dual drugs was also pivotal for IPF therapy.

4. Conclusions

In IPF treatment, the over-activation of inflammatory responses and pro-fibrotic effects lead to unsatisfactory anti-fibrosis efficacy. Herein, we built a nanoengineered immunosuppressive therapeutic (PNCE) which could firstly target MOMCs and then be delivered into IPF lungs, and could be detached sensitively from MOMCs. Hereinto, COL acted on macrophages modulating M1 macrophages into M2 macrophages in innate immune responses, thereby further enhancing the suppressing effect of NIN on fibroblast activation, and improving the efficacy of IPF treatment.

In conclusion, we confirmed that in the case of the immune inhibitor COL, the anti-fibrosis ability of NIN had a significant enhancement. This strategy showed excellent results and strongly supports the use of COL to enhance IPF treatment. Modulation of the macrophage polarization and reduction of fibroblast over-proliferation could significantly downregulate collagen accumulation, improving the IPF treatment efficacy. These results suggested that the nanoengineered immunosuppressive therapeutic with a co-delivery immune regulator and anti-fibrotic drugs is an effective strategy to improve the therapeutic efficacy for IPF.

Conflicts of interest

The authors declare no conflict of interest.

Acknowledgements

This work was financially supported by the National Science and Technology Major Project (2017YFA0205400), the National Natural Science Foundation of China (81773667, 81573369 and 81430082), and the NSFC Projects of International Cooperation and Exchanges (81811540416). This work was also supported by the Double first-class project (CPU2018GY06) and the Priority Academic Program Development of Jiangsu Higher Education Institutions. A Project Funded by the Priority Academic Program Development of Jiangsu Higher Education Institutions. The authors thank the Cellular and Molecular Biology Center of China Pharmaceutical University for assistance with confocal microscopy work.

Notes and references

- 1 M. Selman and A. Pardo, The epithelial/fibroblastic pathway in the pathogenesis of idiopathic pulmonary fibrosis, *Am. J. Respir. Cell Mol. Biol.*, 2003, **29**, S93–S97.
- 2 T. S. Blackwell, A. M. Tager, Z. Borok, B. B. Moore, D. A. Schwartz, K. J. Anstrom, Z. Bar-Joseph, P. Bitterman, M. R. Blackburn, W. Bradford, K. K. Brown, H. A. Chapman, H. R. Collard, G. P. Cosgrove, R. Deterding, R. Doyle, K. R. Flaherty, C. K. Garcia, J. S. Hagood, C. A. Henke, E. Herzog, C. M. Hogaboam, J. C. Horowitz, T. E. King, J. E. Loyd, W. E. Lawson, C. B. Marsh, P. W. Noble, I. Noth, D. Sheppard, J. Olsson, L. A. Ortiz, T. G. O'Riordan, T. D. Oury, G. Raghu, J. Roman, P. J. Sime, T. H. Sisson, D. Tschumperlin, S. M. Violette, T. E. Weaver, R. G. Wells, E. S. White, N. Kaminski, F. J. Martinez, T. A. Wynn, V. J. Thannickal and J. P. Eu, Future directions in idiopathic pulmonary fibrosis research an NHLBI workshop report, *Am. J. Respir. Crit. Care Med.*, 2014, **189**, 214–222.
- 3 F. Dudbridge, R. J. Allen, N. A. Sheehan, A. F. Schmidt, J. C. Lee, R. G. Jenkins, L. V. Wain, A. D. Hingorani and R. S. Patel, Adjustment for index event bias in genome-wide association studies of subsequent events, *Nat. Commun.*, 2019, **10**, 1561.
- 4 J. Duffield, S. M. Lupher, V. J. Thannickal and T. A. Wynn, Host responses in tissue Repair and fibrosis, *Annu. Rev. Pathol.: Mech. Dis.*, 2013, **8**, 241–276.
- 5 S. Cannito, E. Novo and M. Parola, Therapeutic pro-fibrogenic signaling pathways in fibroblasts, *Adv. Drug Delivery Rev.*, 2017, **121**, 57–84.
- 6 G. M. Hunninghake, Interstitial lung abnormalities: erecting fences in path towards advanced pulmonary fibrosis, *Thorax*, 2019, **74**, 506–511.
- 7 J. Rajchgot and M. B. Stanbrook, Combination nintedanib and pirfenidone for treatment of idiopathic pulmonary fibrosis, *Am. J. Respir. Crit. Care Med.*, 2018, **198**, 1105.
- 8 K. E. Hostettler, E. Papakonstantinou, J. Klagas, G. Karakiulakis, J. Zhong, M. Tamm, D. Lardinois and M. Roth, Anti-fibrotic effects of nintedanib (bibf 1120) in

- primary human lung fibroblasts derived from patients with idiopathic pulmonary fibrosis and from non-fibrotic controls, *Am. J. Respir. Crit. Care Med.*, 2013, **184**, A3374.
- 9 L. R. Richeldi, M. du Bois, G. Raghu, A. Azuma, K. K. Brown, U. Costabel, V. Cottin, K. R. Flaherty, D. M. Hansell, Y. Inoue, D. S. Kim, M. Kolb, A. G. Nicholson, P. W. Noble, M. Selman, H. Taniguchi, M. Brun, F. L. Maulf, M. Girard, S. Stowasser, R. Schlenker-Herceg, B. Disse and H. R. Collard, Efficacy and safety of nintedanib in idiopathic pulmonary fibrosis, *N. Engl. J. Med.*, 2018, **370**, 2071–2082.
 - 10 W. Jiang, X. Wang, O. J. Osborne, Y. J. Du, C. H. Chang, Y. P. Liao, B. B. Sun, J. H. Jiang, Z. X. Ji, R. B. Li, X. S. Liu, J. Q. Lu, S. J. Lin, H. Meng, T. Xia and A. E. Nel, Pro-inflammatory and pro-fibrogenic effects of ionic and particulate arsenide and indium-containing semiconductor materials in the murine lung, *ACS Nano*, 2017, **11**, 1869–1883.
 - 11 J. Y. Chen and S. JoAnne, Bleomycin: towards better therapeutics, *Nat. Rev. Cancer*, 2005, **5**, 102–112.
 - 12 P. W. Noble, C. E. Barkauskas and D. H. Jiang, Pulmonary fibrosis: patterns and perpetrators, *J. Clin. Invest.*, 2012, **122**, 2756–2762.
 - 13 S. S. Liu, X. X. Lv, C. Liu, J. Qi, Y. X. Li, X. Wei, P. K. Li, F. Hua, B. Cui, X. W. Zhang, J. J. Yu, J. M. Yu, F. Wang, S. Shang, C. X. Zhao, X. Y. Hou, Z. G. Yao, P. P. Li and Z. W. Hu, Targeting the transcriptional factor C/EBP β degradation reduces lung fibrosis by restoring activity of the ubiquitin-editing enzyme A20 in macrophages, *Immunity*, 2019, **51**, 522.
 - 14 M. L. Smith, Not all fibrosis is created equally, *Arch. Pathol. Lab. Med.*, 2016, **140**, 221–229.
 - 15 K. K. Kim, M. C. Kugler, P. J. Wolters, L. Robillard, M. G. Galvez, A. M. Brumwell, D. Sheppard and H. A. Chapman, Alveolar epithelial cell mesenchymal transition develops *in vivo* during pulmonary fibrosis and is regulated by the extracellular matrix, *Proc. Natl. Acad. Sci. U. S. A.*, 2006, **103**, 13180–13185.
 - 16 S. I. Rennard, P. B. Bitterman, T. Ozaki, W. N. Rom and R. G. Crystal, Colchicine suppresses the release of fibroblast growth factors from alveolar macrophages *in vitro*. The basis of a possible therapeutic approach to the fibrotic disorders, *Am. Rev. Respir. Dis.*, 1988, **137**, 181–185.
 - 17 T. Misawa, M. Takahama, T. Kozaki, H. Lee, J. Zou, T. Saitoh and S. Akira, Microtubule-driven spatial arrangement of mitochondria promotes activation of the NLRP3 inflammasome, *Nat. Immunol.*, 2013, **14**, 454–460.
 - 18 X. J. Li, H. Guo, H. Y. Duan, Y. L. Yang, J. Meng, J. Liu, C. Wang and H. Y. Xu, Targeting CXCR 4/CXCL 12 axis to improve chemotherapeutics efficiency in acute myeloid leukemia treatments by synthesized peptide E5, *Nanomedicine*, 2018, **14**, 1764–1765.
 - 19 R. M. Strieter, B. N. Gomperts and M. P. Keane, The role of CXC chemokines in pulmonary fibrosis, *J. Clin. Invest.*, 2007, **117**, 549–556.
 - 20 T. Ji, J. Lang, J. Wang, R. Cai, Y. Zhang, F. Qi, L. Zhang, X. Zhao, W. Wu, J. Hao, Z. Qin, Y. Zhao and G. Nie, Designing liposomes to suppress extracellular matrix expression to enhance drug penetration and pancreatic tumor therapy, *ACS Nano*, 2017, **11**, 8668–8678.
 - 21 M. Kuwana, Y. Okazaki, H. Kodama, K. Izumi, H. Yasuoka, Y. Ogawa, Y. Kawakami and Y. Ikeda, Human circulating CD¹⁴⁺ monocytes as a source of progenitors that exhibit mesenchymal cell differentiation, *J. Leukocyte Biol.*, 2003, **74**, 833–845.
 - 22 N. Seta and M. Kuwana, Derivation of multipotent progenitors from human circulating CD¹⁴⁺ monocytes, *Exp. Hematol.*, 2010, **38**, 557–563.
 - 23 F. Xia, J. Niu, Y. Hong, C. Li, W. Cao, L. Wang, W. Hou, Y. Liu and D. Cui, Matrix metalloproteinase 2 targeted delivery of gold nanostars decorated with IR-780 iodide for dual-modal imaging and enhanced photothermal/photodynamic therapy, *Acta Biomater.*, 2019, **89**, 289–299.
 - 24 L. Wang, X. X. Niu, Q. L. Song, J. J. Jia, Y. W. Hao, C. X. Zheng, K. L. Ding, H. F. Xiao, X. X. Liu, Z. Z. Zhang and Y. Zhang, A two-step precise targeting nanoplatfor for tumor therapy via the alkyl radicals activated by the microenvironment of organelles, *J. Controlled Release*, 2020, **318**, 197–209.
 - 25 G. Deng, Z. Sun, S. Li, X. Peng, W. Li, L. Zhou, Y. Ma, P. Gong and L. Cai, Cell-membrane immunotherapy based on natural killer cell membrane coated nanoparticles for the effective inhibition of primary and abscopal tumor, *ACS Nano*, 2018, **12**, 12096–12108.
 - 26 Y. W. He, R. X. Li, H. C. Li, S. Y. Zhang, W. T. Dai, Q. Wu, L. X. Jiang, Z. C. Zheng, S. Shen and X. Chen, Erythroliosomes: integrated hybrid nanovesicles composed of erythrocyte membranes and artificial lipid membranes for pore-forming toxin clearance, *ACS Nano*, 2019, **13**, 4148–4159.
 - 27 A. Parodi, N. Quattrocchi, A. L. Van de Ven, C. Chiappini, M. Evangelopoulos, J. O. Martinez, B. S. Brown, S. Z. Khaled, I. K. Yazdi, M. V. Enzo, L. Isenhardt, M. Ferrari and E. Tasciotti, Biomimetic functionalization with leukocyte membranes imparts cell like functions to synthetic particles, *Nat. Nanotechnol.*, 2013, **8**, 61–68.
 - 28 E. N. Arwert, A. S. Harney, D. Entenberg, Y. Wang, E. Sahai, J. W. Pollard and J. S. Condeelis, A unidirectional transition from migratory to perivascular macrophage is required for tumor cell intravasation, *Cell Rep.*, 2018, **23**, 1239–1248.
 - 29 S. Habringer, P. Herhaus, M. Schottelius, C. Lapa, R. Istvanffy, K. Gotze, K. Steiger, B. Vick, C. Peschel, R. Oostendorp, I. Eremias, H. J. Wester, G. U. Grigoleit and U. Keller, Peptide-receptor radiotherapy with CXCR4-targeting pentixather reduces leukemia burden in acute leukemia PDX and patients, *Blood*, 2016, **128**, 4055.
 - 30 K. Griffiths, O. Dolezal, B. Cao, S. K. Nilsson, H. B. See, K. D. G. Pflieger, M. Roche, P. R. Gorry, A. Pow, K. Viduka, K. Lim, B. G. C. Lu, D. H. C. Chang, T. Murray-Rust, M. Kvensakul, M. A. Perugini, C. Dogovski, M. Doerflinger, Y. Zhang, K. Parisi, J. L. Casey, S. D. Nuttall and M. Foley, I-bodies: human single domain antibodies that antagonize

- chemokine receptor CXCR4, *J. Biol. Chem.*, 2016, **291**, 12641–12657.
- 31 K. Tsujino, Y. Takeda, T. Arai, Y. Shintani, R. Inagaki, H. Saiga, T. Iwasaki, S. Tetsumoto, Y. Jin, S. Ihara, T. Minami, M. Suzuki, I. Nagatomo, K. Inoue, H. Kida, T. Kijima, M. Ito, M. Kitaichi, Y. Inoue, I. Tachibana, K. Takeda, M. Okumura, M. E. Hemler and A. Kumanogoh, Tetraspanin CD 151 protects against pulmonary fibrosis by maintaining epithelial integrity, *Am. J. Respir. Crit. Care Med.*, 2012, **186**, 170–180.
- 32 K. Byun, Y. Yoo, M. Son, J. Lee, G. B. Jeong, Y. M. Park, G. H. Salekdeh and B. Lee, Advanced glycation end-products produced systemically and by macrophages: a common contributor to inflammation and degenerative diseases, *Pharmacol. Ther.*, 2017, **177**, 44–55.
- 33 T. Bärnthaler, A. Theiler, D. Zabini, S. Trautmann, S. P. Elvira, I. Lanz, W. Klepetko, K. Sinn, H. Flick, S. Scheidl, D. Thomas, H. Olschewski, G. Kwapiszewska, R. Schuligoi and A. Heinemann, Inhibiting eicosanoid degradation exerts antifibrotic effects in a pulmonary fibrosis mouse model and human tissue, *J. Allergy Clin. Immunol.*, 2019, **145**, 818–833.
- 34 M. I. Suwara, L. A. Borthwick, J. Mann, A. J. Fisher and D. A. Mann, S120 IL-1 is a key epithelial alarmin which promotes fibroblast activation, *Thorax*, 2010, **65**, 55–56.
- 35 G. C. Smaldone, Repurposing of gamma interferon via inhalation delivery, *Adv. Drug Delivery Rev.*, 2018, **133**, 87–92.
- 36 G. Savary, E. Dewaeles, S. Diazzi, M. Buscot, N. Nottet, J. Fassy, E. Courcot, I. S. Henaoui, J. Lemaire, N. Martis, H. C. Van, N. Pons, V. Magnone, S. Leroy, V. Hofman, L. Plantier, K. Lebrigand, A. Paquet, C. L. Lino, G. Vassaux, P. Hofman, A. Günther, B. Crestani, B. Wallaert, R. Rezzonico, T. Brousseau, F. Glowacki, S. Bellusci, M. Perrais, F. Broly, P. Barbry, C. H. Marquette, C. Cauffiez, B. Mari and N. Pottier, The long noncoding RNA DNMT3OS is a reservoir of fibromirs with major functions in lung fibroblast response to TGF- β and pulmonary fibrosis, *Am. J. Respir. Crit. Care Med.*, 2019, **200**, 2066.
- 37 L. J. Celada, J. A. Kropski, J. D. Herazo-Maya, W. F. Luo, A. Creecy, A. T. Abad, O. S. Chioma, G. Lee, N. E. Hassell, G. I. Shaginurova, Y. F. Wang, J. E. Johnson, A. Kerrigan, W. R. Mason, R. P. Baughman, G. D. Ayers, G. R. Bernard, D. A. Culver, C. G. Montgomery, T. M. Maher, P. L. Molyneaux, I. S. Noth, E. Mutsaers, C. M. Prele, R. S. Peebles, D. C. Newcomb, N. Kaminski, T. S. Blackwell, L. V. Kaer and W. P. Drake, PD-1 up-regulation on CD⁴⁺ T cells promotes pulmonary fibrosis through STAT3-mediated IL-17A and TGF- β 1 production, *Sci. Transl. Med.*, 2018, **10**, eaar8356.